

The multi-dimensional limiters for discontinuous Galerkin method on unstructured grids

Wanai Li, Yu-Xin Ren

Corresponding author: ryx@tsinghua.edu.cn

Department of engineering mechanics, Tsinghua university, Beijing, China.

Abstract: Accuracy-preserving and non-oscillatory shock-capturing technique is the bottle neck in the development of discontinuous Galerkin method. Inspired by the success of the k-exact WENO limiters for high order finite volume methods, this paper generalize the k-exact WENO limiter to discontinuous Galerkin methods. Also several improvements are put forward to keep the compactness and high-order accurate properties of DG method. The resulting schemes are easy to implement and effective in capturing the shock waves. Some standard cases are performed to validate the accuracy and robustness of the proposed limiters for the DG methods.

Keywords: Accuracy-Preserving, Limiters, Discontinuous Galerkin Method, Unstructured grids.

1 Introduction

High order accurate numerical methods have been an active research area in CFD community recently. Compared to lower order methods, they can provide more reliable results especially in flows with a broad range of length scales. In applications such as the direct numerical simulation (DNS) and large eddy simulation (LES) of turbulent flows and computational aero-acoustics (CAA), high order methods have shown promise in handling such cases. The design of high order methods on unstructured grids is extremely demanding due to the complexities of the geometries, and as the result, they are not so mature. Ongoing studies are still carried out on the continuous development of such kind of schemes including the finite volume (FV) method [1], spectral volume/difference method [13], discontinuous Galerkin (DG) method [2], $P_N P_M$ method [4] and correction procedure via reconstruction (CPR) method [14].

Among these methods, the DG methods are widely investigated for its flexibility in handling various types of grids, compact stencil support, strong conservation and stability properties. However, a number of problems in the DG methods need to be studied further. And one of these problems, probably the most challenging one, is how to suppress the spurious oscillations near the discontinuities and keep the high order accuracy away from discontinuities. One popular way for treating these discontinuities is the reconstruction and limiting technique. Zhu&Qiu [17] applied the high order WENO limiters with multiple reconstruction [6] in Runge-Kutta DG schemes. And to be more compact, the hermite WENO limiters using the first derivatives are also constructed for DG schemes [16]. Kim et al [10] also extended the successful MLP in FV methods to MLP-DG limiters. Xu et al [11, 12] proposed the hierarchical/point hierarchical reconstruction with WENO-like limiter to make the limiter in DG method be compact. Whereas the design of robust, accurate and oscillation-free shock-capturing technique still remains an open question for the DG methods.

Based on the k-exact WENO limiters for the high-order FV methods [8], a new limiting procedure will be proposed in this paper to provide a simple yet efficient limiter for the DG methods. Compared to the WENO/hermite WENO limiters [17, 16], the limiters introduced in this paper are simpler and keep the compactness property of DG methods. These characteristics are achieved by improving the k-exact WENO limiters in the following aspects. Firstly the WENO candidate limiting polynomials are provided using the secondary reconstruction which only uses the information on face-neighbor cells. Secondly, to keep the sub-cell resolution property of DG methods, the WENO weighted procedure needs to be designed more accurately and efficiently. The outlines of the remainder of the paper are as follows. In Section 2 we described the framework for the discontinuous Galerkin methods in solving Euler equations. The procedure

for constructing the limiters is presented in Section 3. The test cases are simulated in Section 4. And the conclusions are given in Section 5.

2 Framework of the discontinuous Galerkin methods

This section describes the discretization of the discontinuous Galerkin schemes on unstructured grids. The equations are the Euler equations governing the unsteady compressible inviscid flow, written as

$$\frac{\partial U}{\partial t} + \frac{\partial F}{\partial x} + \frac{\partial G}{\partial y} = 0, \quad (1)$$

where U is the vector of the conservative variables given as $U = (\rho, \rho u, \rho v, \rho E)^T$. The detailed formulations of the flux terms are well-known and are omitted here for brevity.

The discretization of Eq. (1) using the discontinuous Galerkin method is in terms of the weak formulation of Eq. (1),

$$\int_{\Omega_i} \frac{\partial U}{\partial t} W d\Omega + \oint_{\partial\Omega_i} \widehat{F}_n \cdot \vec{n} W ds - \int_{\Omega_i} \vec{F}_n \cdot \nabla W d\Omega = 0, \quad \vec{F}_n = (F, G), \quad (2)$$

where $\partial\Omega_i$ denotes the boundary of Ω_i , \vec{n} is the unit outward normal vector to the boundary, and W is the test function.

We assume that the approximate distribution $U^h(\vec{x}, t)$ inside the cell is a k -th order polynomial, which can be expressed on a series of zero-mean basis $\phi_i(x, y) = \{\varphi_l(x, y)\}$,

$$U^h(\vec{x}, t) = \sum_{l=0}^K U_i^l(t) \varphi_{l,i}(\vec{x}), \quad (3)$$

where $K = (k+1)(k+2)/2 - 1$, U_i^l denotes the degree of freedom (DOF) and U_i^0 is the cell-averaged value. To reduce the stiffness of the discretization equations, the local hierarchical orthogonal basis is employed. By taking the basis function to be the test function and substituting the approximate solution (3) into Eq. (2), the DOFs can be updated by

$$\frac{\partial U_i^l}{\partial t} \int_{\Omega_i} (\varphi_{l,i})^2 d\Omega + \oint_{\partial\Omega_i} \widehat{F}_n \cdot \vec{n} \varphi_{l,i} ds - \int_{\Omega_i} \vec{F}_n(U^h) \cdot \nabla \varphi_{l,i} d\Omega = 0, \quad l = 0, \dots, K.$$

The interface flux is computed using the an approximated Riemann solver, for which the HLL Riemann solver [5] is adopted in this paper. The volume and surface integrals are calculated using $2k$ and $2k+1$ order accurate Gauss quadrature rules. This semi-discrete system is integrated using the third order Runge-Kutta scheme.

3 The construction of the multi-dimensional limiters

The most challenging work for designing limiters for the DG method is to keep all the merits of the DG methods, e.g., compactness and high-order accuracy properties. Compared to the FV methods, DG methods have more DOFs inside the cell which makes DG achieve higher resolutions. However, this also bring in more difficulties in treating the discontinuities. The multi-dimensional limiters proposed in this section try to keep those merits of DG methods.

Since the limiters are generalized from the k-exact WENO limiters for high order FV schemes [8], a brief introduction will be given to k-exact WENO limiters first. In our previous paper [8], we constructed the secondary reconstruction (SR) procedure to provide candidate polynomials for the WENO limiters. With the SR method, the limiting stencils are clearly specified as shown in Fig. 1 and the candidate polynomials are easily computed. With the polynomials reconstructed using the k-exact and secondary reconstructions, we use the WENO weights to average all these polynomials. These two steps make the k-exact WENO

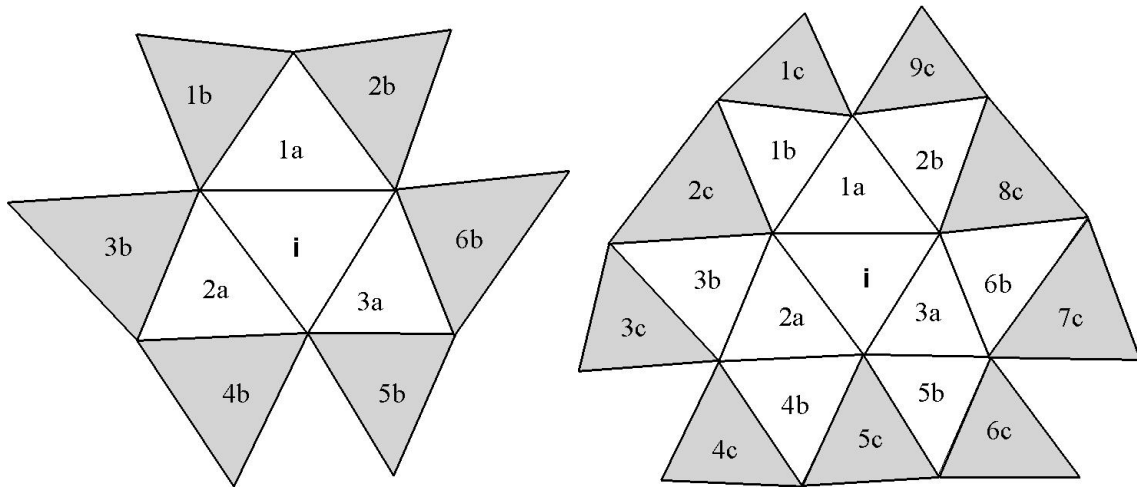


Figure 1: The limiting stencils of FV method. Left: 3rd order; right: 4th order.

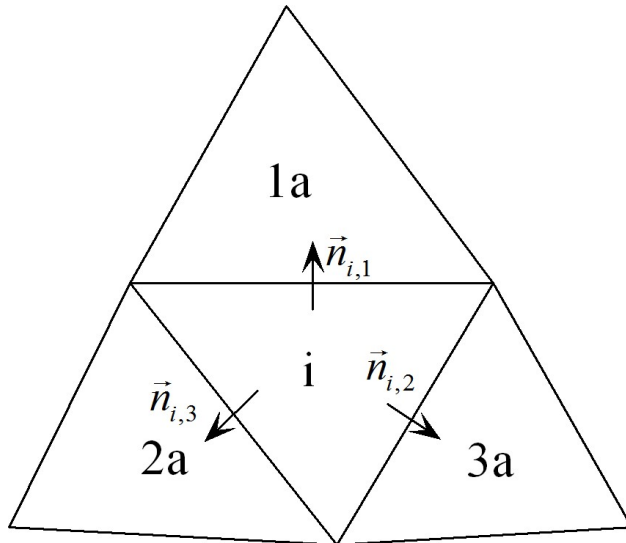


Figure 2: The limiting stencils of DG method. $T_i = \{1a, 2a, 3a\}$.

limiters more efficient than traditional WENO limiters with multiple reconstructions. To generalize the k-exact WENO limiters to DG methods, the following two steps need to improve. 1) In the finite volume k-exact WENO scheme, the cells performing the SR is compact. In the limiting procedure of the DG method, only the face neighbors shown in Fig. 2 will be used to carry out the SR which makes the limiting procedure compact. In the DG method, the SR will be carried out in terms of the hierarchical orthogonal basis instead of the simple Taylor basis. 2) The parameters in the WENO limiting procedure is adjusted for the DG methods to improve the performance of the limiter.

Now we give detail descriptions about the two procedure below.

3.1 The secondary reconstruction

The secondary reconstruction is very simple and straightforward. Assuming cell j is a face-neighbor of cell i , we define the secondary reconstruction of cell i using the information of cell j as $u_{i,j}(\vec{x})$. $u_{i,j}(\vec{x})$ is constructed

by solving

$$\begin{aligned} \int_{\Omega_i} u_{i,j}(\vec{x}) d\Omega &= u_i^0 \|\Omega_i\|, \\ \int_{\Omega_j} u_{i,j}(\vec{x}) \varphi_{l,j} d\Omega &= \int_{\Omega_j} u_j(\vec{x}) \varphi_{l,j} d\Omega = u_j^k \int_{\Omega_j} (\varphi_{l,j})^2 d\Omega, \quad l = 1, \dots, K, j \in T_i = \{1a, 2a, 3a\}, \end{aligned} \quad (4)$$

where $\|\Omega_i\|$ is the area in Ω_i and u_i^0 is the cell average of the solution on cell i . The limiting stencils are shown in Fig. 2. It is clear that the secondary reconstruction is conservative and uses only information on current cell and its face-neighbors.

To obtain the unknowns $u_{i,j}(\vec{x})$, there is no need to implement the integration and solve the linear equations. Following a similar idea in [9], we first write $u_{i,j}(\vec{x})$ using the orthogonal basis in Ω_i , i.e.

$$u_{i,j}(\vec{x}) = u_i^0 + \sum_{l=1}^K u_{i,j}^l \varphi_{l,i}(\vec{x}). \quad (5)$$

It is obviously that the first equation in Eq. (4) is automatically satisfied. According to the construction procedure of hierarchical orthogonal polynomials, the expression of $\varphi_{l,i}$ can be expressed only by the basis $\varphi_{k,j}$, $k = 0, \dots, l$, namely $\varphi_{l,i}(\vec{x}) = \sum_{k=0}^l c_{k,l} \varphi_{k,j}(\vec{x})$. Substitute it into Eq. (5) and we have

$$\begin{aligned} u_{i,j}(\vec{x}) &= u_i^0 + \sum_{l=1}^K \left(u_{i,j}^l \sum_{k=0}^l c_{k,l} \varphi_{k,j}(\vec{x}) \right) \\ &= \left(u_i^0 + \sum_{l=1}^K u_{i,j}^l c_{0,l} \varphi_{0,j}(\vec{x}) \right) + \sum_{k=1}^K \left(\sum_{l=1}^K u_{i,j}^l c_{k,l} \right) \varphi_{k,j}(\vec{x}). \end{aligned}$$

According to the second equation in Eq. (4),

$$\sum_{l=1}^K u_{i,j}^l c_{k,l} = u_j^k, \quad k = 1, \dots, K.$$

Then the unknowns $u_{i,j}^l$, $l = 1, \dots, K$ can be solved and the candidate polynomial $u_{i,j}(\vec{x})$ is obtained.

3.2 The WENO limiting procedure

According to above procedure, four candidate polynomials can be obtained, namely $u_i(\vec{x}), u_{i,j}(\vec{x}), j \in T_i = \{1a, 2a, 3a\}$. The next step is applying WENO procedure on the four polynomials. To ease the presentation below, these polynomials are denoted as $u_{i,k}(\vec{x}), k = 0, \dots, Nl, Nl = 3$, where $u_{i,0}(\vec{x})$ represents the polynomial $u_i(\vec{x})$, and $u_{i,k}(\vec{x}), k = 1, \dots, Nl$ represents the polynomials $u_{i,j}(\vec{x})$. The final reconstruction polynomials are obtained by the weighted average of these polynomials. Specifically, $u_{i,k}(\vec{x}), k = 0, \dots, Nl$ are firstly transformed to the characteristic space and the corresponding characteristic polynomials are denoted with $V_{i,k}(\vec{x})$, using

$$V_l^m = (R^m)^{-1} U_{i,l}, \quad l = 0, \dots, Nl. \quad (6)$$

where R^m is the matrix of right eigenvectors of the Jacobian matrix of Eq. (1) associated with the direction \vec{n}_m . For the triangular control volume, $m = 1, 2, 3$. Then the smoothness indicators are computed using

$$\beta_k = \sum_{m+n=1}^K h^{m+n-1} \iint_{\Omega_i} \left(\frac{\partial^{m+n} v_{i,k}}{\partial x^m \partial y^n} \right)^2 dx dy,$$

where $v_{i,k}$ is the component of $V_{i,k}$ and h is the dimension of cell Ω_i . In terms of these smoothness indicators, the WENO weight of each candidate reconstruction is determined by

$$w_k = \frac{\alpha_k}{\sum_{l=0}^{Nl} \alpha_l}, \quad \alpha_k = \frac{\lambda_k}{(\varepsilon + \beta_k)^p}$$

Here we choose $p = 2$. $\varepsilon = 10^{-8}$ is a small positive number to avoid possible division by zero, and λ_k is the linear weight. Following the same reasoning of [3], it is beneficial to emphasize the contribution of the primary reconstruction. Therefore, λ_k is computed by

$$\lambda_k = \begin{cases} \lambda_0, & k = 0, \\ 1, & \textit{else}. \end{cases}$$

λ_0 can be chosen as 1000 and 10000 in our computation. In Section 4, we will give numerical examples on the influence of this parameter. Unless otherwise specified, λ_0 is set to be 1000. The final polynomial for the cell Ω_i would be the weighted summation of all candidate polynomials,

$$\tilde{v}^m(\vec{x}) = \sum_{l=0}^{Nl} w_l \cdot v_{i,l}^m(\vec{x}).$$

The limited polynomials using characteristic variables are then transformed back to the conservative variables which are denoted by $\tilde{u}_i^m(\vec{x})$. Therefore, we obtain 3 sets of limited polynomials. From the point of view of practical applications, it is better to have a unique reconstruction polynomial since there is source term in the DG discretization. In the present paper, $\tilde{u}_i^m(\vec{x})$, $m = 1, 2, 3$ are further limited using

$$\tilde{u}_i(\vec{x}) = \sum_{m=1}^3 w_{\bar{n}_{i,m}} \tilde{u}_i^m(\vec{x})$$

where $w_{\bar{n}_{i,m}}$ is the WENO weight for $\tilde{u}_i^m(\vec{x})$ in the three directions. And $\tilde{u}_i(\vec{x})$ is the final limited polynomial.

The limiting procedure proposed in this section only uses information in face-neighbor cell, thus it keeps the compact property of DG methods. And from the numerical examples shown in Section 4, it can achieve high order accuracy in smooth region and suppress the oscillations near the discontinuities. Since the discontinuities are local phenomenon in the flow field, the shock detector is used in time-consuming cases. In this paper, the parameter-free KXRCF shock detector [7] is adopted.

4 Numerical examples

In this section, we apply the DG methods with the multi-dimensional limiters proposed in the previous sections to solve a number of 2D test cases. These test cases are used to test the accuracy, robustness, resolution and shock capturing capability of the proposed schemes. In all test cases, the CFL number is taken as 0.8. There are some test cases for which the solutions are one-dimensional in nature. They are nevertheless solved on two-dimensional domains.

4.1 Linear advection

The first two-dimensional test case on unstructured grids is the linear initial-boundary value problem

$$\begin{aligned} u_t + u_x + u_y &= 0, 0 \leq x \leq 2, t > 0 \\ u(x, y, 0) &= u_0(x, y), \\ u(x, y, 2) &= u(x, y, 2) \end{aligned}$$

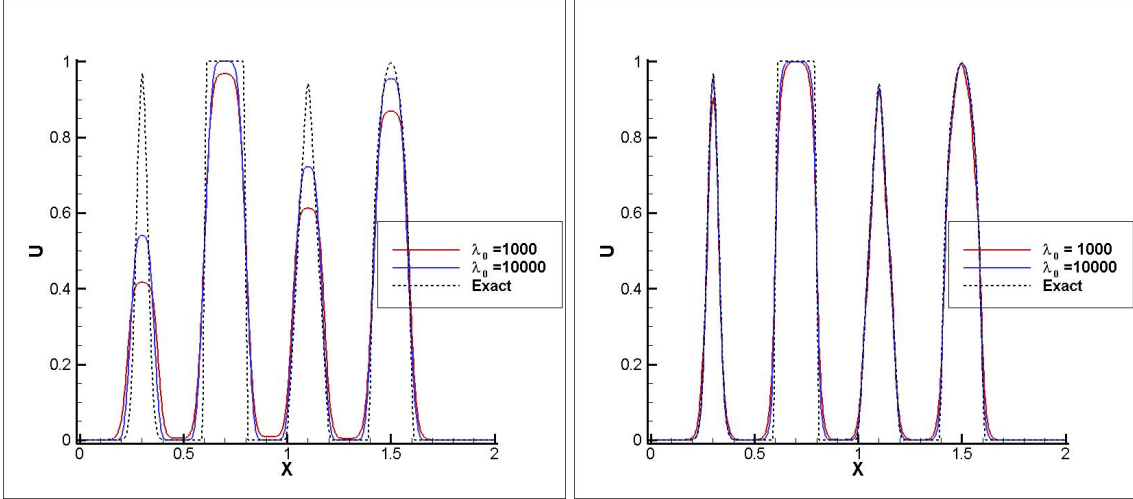


Figure 3: Solution for linear advection problem at $T = 16$. Left: 2nd order; right: 3rd order.

with following initial condition

$$u_0(x) = \begin{cases} \frac{1}{6} (G(x, \beta, z - \delta) + G(x, \beta, z + \delta) + 4G(x, \beta, z)), & 0.2 \leq x \leq 0.4, \\ 1, & 0.6 \leq x \leq 0.8, \\ 1 - |10(x - 0.1)|, & 1 \leq x \leq 1.2, \\ \frac{1}{6} (G(x, \beta, z - \delta) + G(x, \beta, z + \delta) + 4G(x, \beta, z)), & 1.4 \leq x \leq 1.6, \\ 0, & \text{otherwise} \end{cases}$$

$$G(x, \beta, z) = e^{-\beta(x-z)^2}$$

$$F(x, \alpha, a) = \sqrt{\max(1 - \alpha^2(x - a)^2, 0)}$$

where $a = 0.5, z = -0.7, \delta = 0.005, \alpha = 10$, and $\beta = \frac{\log 2}{36\delta^2}$. The initial profile consists of a combination of Gaussians, a square pulse, a sharp triangle, and a combination of half-ellipse. The computational domain is taken as $[0, 2] \times [0, 0.4]$, and periodic boundary conditions are used. The grids used for computation are uniform triangular grids with grid size $h = 1/100$. The solution is computed to $T = 16$ using 2nd and 3rd order DG methods with different λ_0 . Fig. 3 compares different DG methods performance. For both $\lambda = 1000$ and 10000 , the 2nd and 3rd order DG methods can capture the discontinuities without oscillations. Larger λ_0 and high order schemes can greatly increase the accuracy.

4.2 Isentropic vortex

The isentropic vortex transport problem [6] is used to examine the accuracy of the numerical scheme in computing multi-dimensional flow without shock waves. The mean flow is $\rho = 1, p = 1$, and $(u, v) = (0, 0)$. We add, to mean flow, an isentropic vortex expressed by the following perturbations,

$$(\delta u, \delta v) = \frac{\varepsilon}{2\pi} e^{0.5(1-r^2)} (-\bar{y}, \bar{x})$$

$$\delta T = -\frac{(\gamma - 1)\varepsilon^2}{8\gamma\pi^2} e^{1-r^2}, \quad \delta S = 0$$

with $(\bar{x}, \bar{y}) = (x - 5, y - 5), r^2 = \bar{x}^2 + \bar{y}^2$, and the vortex strength $\varepsilon = 5$.

We compute the solution at $t = 2.0$ to test the accuracy of the proposed schemes without the shock detector. The grids used for test are the uniform grids in the same test case in [8]. The numerical results are shown in Table 1 for the unlimited DG scheme and DG scheme with limiters. For the WENO limiter, λ_0 is set to be 1000 and no shock detector is used. In terms of convergence rate of the density, all schemes can achieve their theoretical values in terms of both L_1 and L_∞ norm. From both Table 1 and Fig. 4, we can

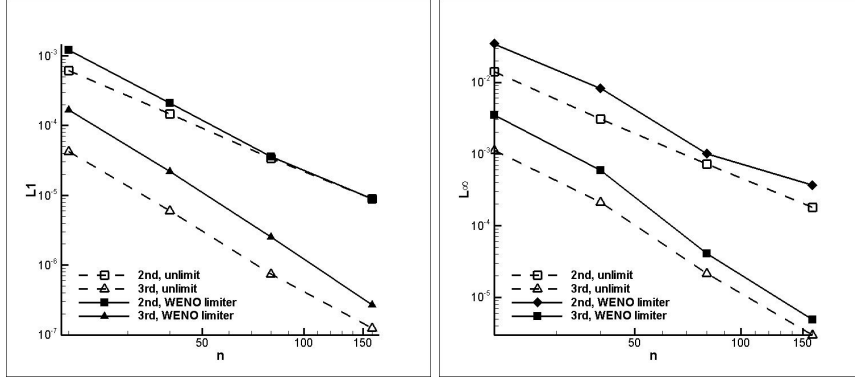


Figure 4: Accuracy for isentropic vortex problem for DG method with/without limiter.

find that the errors using 2nd order DG scheme with limiter is only a bit lower than that using unlimited one, while errors using 3rd order DG scheme with limiter are about two times that using the unlimited one. Overall the DG schemes with limiters can keep the orders unchanged but more dissipative than the unlimited one.

Table 1: Accuracy comparison between unlimited DG and DG with WENO limiter.

	Scheme	Grid	L_1 error	Order	L_∞ error	Order
Unlimited DG	2nd order	20	6.20E-04		1.40E-02	
		40	1.48E-04	2.07	3.10E-03	2.17
		80	3.41E-05	2.12	7.22E-04	2.10
		160	8.95E-06	1.93	1.80E-04	2.00
	3rd order	20	4.21E-05		1.12E-03	
		40	5.97E-06	2.82	2.12E-04	2.40
		80	7.45E-07	3.00	2.13E-05	3.32
		160	1.24E-07	2.59	2.97E-06	2.84
WENO limiter	2nd order	20	1.20E-03		3.47E-02	
		40	2.12E-04	2.51	8.21E-03	2.08
		80	3.58E-05	2.57	1.01E-03	3.02
		160	8.90E-06	2.01	3.70E-04	1.45
	3rd order	20	1.69E-04		3.49E-03	
		40	2.19E-05	2.95	5.92E-04	2.56
		80	2.52E-06	3.12	4.10E-05	3.85
		160	2.70E-07	3.22	4.85E-06	3.08

4.3 Lax tube problem

The Lax tube problem is solved to test the non-oscillation property of the 2nd and 3rd order DG schemes. The initial data are

$$(\rho, u, p)(\vec{x}) = \begin{cases} (\rho_L, u_L, p_L) & \text{if } x \leq 0.5 \\ (\rho_R, u_R, p_R) & \text{if } x > 0.5 \end{cases}$$

where left and right states are

$$\begin{aligned} (\rho_L, u_L, p_L) &= (0.445, 0.698, 3.528), \\ (\rho_R, u_R, p_R) &= (0.5, 0., 0.571). \end{aligned}$$

The computational domain is $[0, 1] \times [0, 0.2]$ filled by uniform triangular grids the same as Section 4.1 with grid size $h = 1/200$. We output the solution at $T = 0.1$. As shown in the first subfigure in Fig. 5, no oscillations or overshoots occur near the shock or contact discontinuity for 2nd DG scheme with limiters, and the limiting

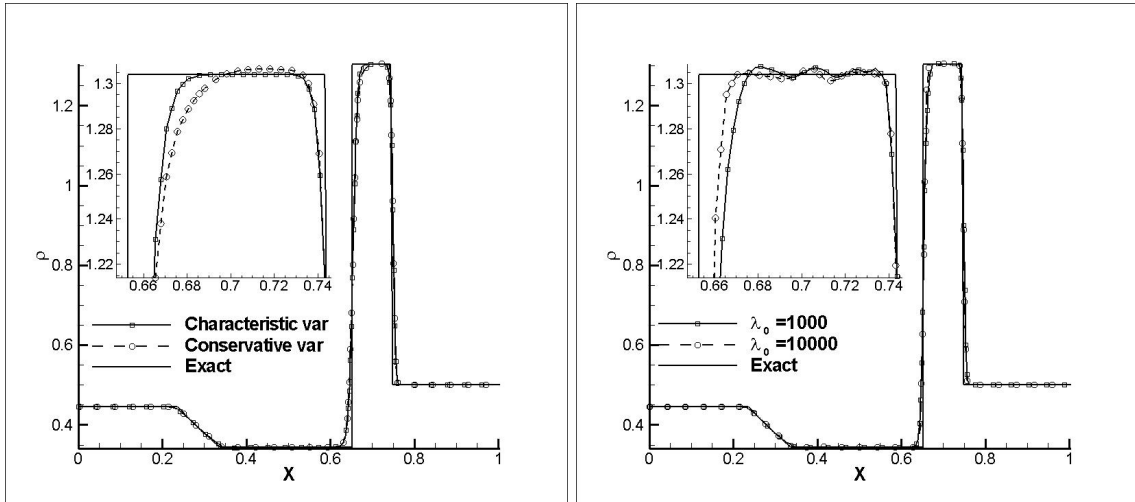


Figure 5: Solution for Lax tube problem. Left: 2nd order; right: 3rd order.

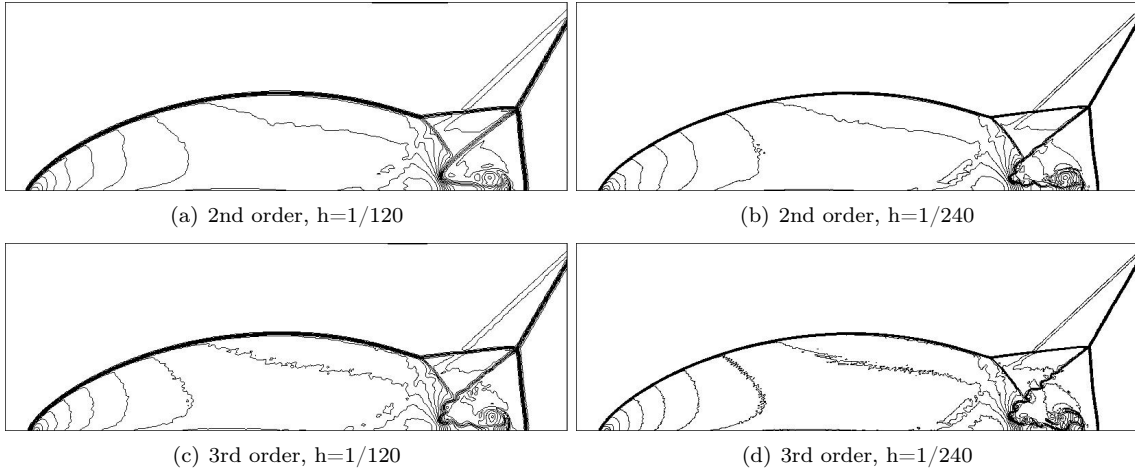


Figure 6: Comparison of density contours for double Mach reflection. Thirty equally spaced contour lines from $\rho = 2.0$ to 21.7 .

with characteristic variables can greatly increase the resolutions near the contact discontinuities. From the second subfigure in Fig. 5 using the 3rd order DG scheme with limiters, small noises are observed in the smooth region but they are not so obvious for both $\lambda_0 = 1000$ and 10000 .

4.4 Double Mach reflection

One of the popular test cases for high-resolution schemes is the double Mach reflection problem. The whole computational domain is $[0, 4] \times [0, 1]$ with the uniform grids. The wall is located at the bottom of the computational domain beginning at $x = 1/6$. Initially, a right-moving shock with $Ma = 10$ is located at $x = 1/6, y = 0$, inclined 60° with respect to the x-axis. The computation is carried out until $T = 0.2$.

We compute the result on a coarse grid ($h=1/120$) and a fine grid ($h=1/240$) using 2nd and 3rd order DG schemes. According to Fig. 6, no oscillations is observed in the results computed using 2nd order limiters and small noises are found in the results computed using 3rd order limiters. From the triple Mach stem shown in Fig 7, We can clearly see that the 3rd order scheme can capture more complicated flow structure than the 2nd order scheme.

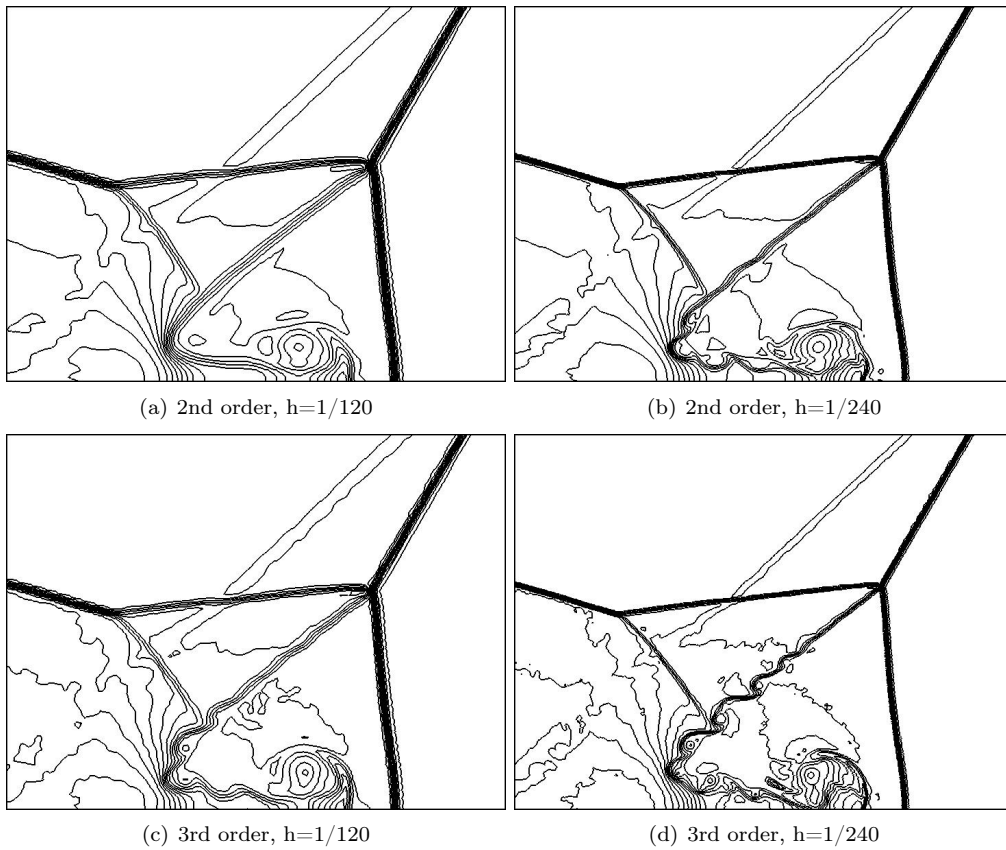


Figure 7: Close-up view around the double Mach stem of Fig. 6.

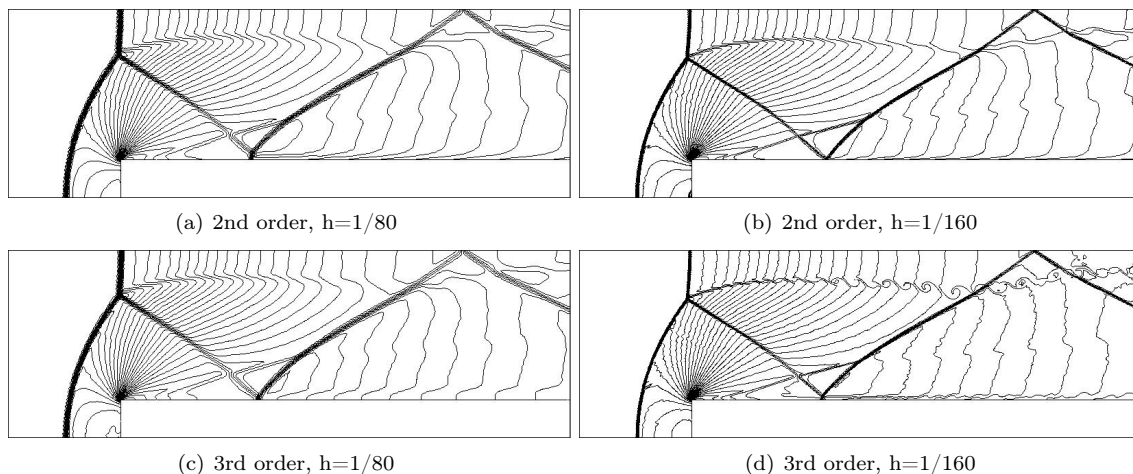


Figure 8: Comparison of density contours for the Mach 3 wind tunnel with a step. Thirty equally spaced contour lines from $\rho = 0.23$ to 6.1.

4.5 A Mach 3 wind tunnel with a step

This is another popular case for high resolution schemes used by P. Woodward [15]. The computational domain is $[0, 3] \times [0, 1]$. The corner of the step is located at $(x, y) = (0.6, 0.2)$. The initial conditions are $(\rho, u, v, p) = (1.4, 3, 0, 1)$ which stand for a Mach 3 uniform flow impacting the step at the initial time.

To avoid the over expansion at the corner, the grids near the corner of wind tunnel are refined as showed in the same case in [8]. The numerical solutions are computed on both a coarse grid ($h = 1/80$) and a fine grid ($h = 1/160$) with the 2nd and 3rd order DG schemes. The results in terms of the density contours are presented in Fig. 8. We can see that 3rd order scheme can resolve the shear layer instability better than 2nd order scheme.

5 Conclusions

We have generalized the k-exact WENO limiters from FV schemes to DG schemes on unstructured grids. To keep the compactness and high order accuracy for DG schemes, two parts in the limiters are improved. The secondary reconstruction only uses information from the face-neighbor cells and is derived using the hierarchical orthogonal basis. The parameters in WENO limiting procedure are given more appropriate values to keep the high resolutions in DG methods. Numerical examples are provided to show that the limiters are robust enough to suppress the oscillations near the shock as well as maintain the accuracy in smooth flow field. Further work will be carried out to improve the limiters to work on arbitrary high order schemes and other types of grids.

References

- [1] T. J. Barth, P. O. Frederickson, Higher order solution of the Euler equations on unstructured grids using quadratic reconstruction, AIAA 90-0013.
- [2] B. Cockburn, CW Shu, Runge-Kutta discontinuous Galerkin methods for convection-dominated problems, *J. Sci. Comp.*, 16(3), 2001.
- [3] M. Dumbser, M. Käser, Arbitrary high order non-oscillatory finite volume schemes on unstructured meshes for linear hyperbolic systems, *J. Comput. Phys.*, 221(2007)693-723.
- [4] M. Dumbser, Arbitrary high order PNPM schemes on unstructured meshes for the compressible Navier-Stokes equations, *Computers & Fluids*, 39 (2010) 60-76.
- [5] A. Harten, P. Lax, B. van Leer, On upstream differencing and Godunov type methods for hyperbolic conservation laws, *SIAM Rev.*, 25(1983)35-61.

- [6] C. Hu, C.W. Shu, Weighted essentially non-oscillatory schemes on triangular meshes, *J. Comput. Phys.*, 150 (1999)97-127.
- [7] L. Krivodonova, et al, Shock detection and limiting with discontinuous Galerkin methods for hyperbolic conservation laws, *Applied Numerical Mathematics* 48(2004)323-338.
- [8] W. Li, Y-X Ren, High order k-exact WENO finite volume schemes for solving gas dynamic Euler equations on unstructured grids, *Int. J. Numer. Meth. Fluids.*, doi: 10.1002/fld.2710.
- [9] W. Li, Y-X Ren, The multi-dimensional limiters for solving hyperbolic conservation laws on unstructured grids II: Extension to high order finite volume schemes, *J. Comput. Phys.*, 231(2012)4053-4077.
- [10] J S Park, C Kim, Higher-order discontinuous Galerkin-MLP methods on triangular and tetrahedral grids. AIAA 2011-3059, 20th AIAA Computational Fluid Dynamics Conference, 27-30 June 2011, Honolulu, Hawaii.
- [11] Z. Xu, Y. Liu, C-W Shu, Hierarchical reconstructin for discontinuous Galerkin methods on unstructured grids with a WENO-type linear reconstruction and partial neighboring cells, *J. Comput. Phys.*, 228(2009)2194-2212.
- [12] Z. Xu, et al, Point-wise hierarchical reconstruction for discontinuous Galerkin and finite volume methods for solving conservation laws, *J. Comput. Phys.*, 230(2011)6843-6865.
- [13] Z.J. Wang, L. Zhang, Y. Liu, Spectral (finite) volume method for conservation laws on unstructured grids IV: extension to two-dimensional systems, *J. Comput. Phys.*, 194(2004)716-741.
- [14] Z.J. Wang and H. Gao, A unifying lifting collocation penalty formulation including the discontinuous Galerkin, spectral volume/difference methods for conservation laws on mixed grids, *J. Comput. Phys.*, 228(2009)8161-8186.
- [15] P. Woodward, P. Colella, The numerical simulation of two-dimensional fluid flow with strong shocks, *J. Comput. Phys.*, 54(1984)115-173.
- [16] J. Zhu, JX Qiu, Hermite WENO schemes and their application as limiters for Runge-Kutta discontinuous Galerkin method III: Unstructured meshes, *J. Sci. Comput.*, 39(2009)293-321.
- [17] J. Zhu, JX Qiu, CW Shu, M. Dumbser, Runge-Kutta discontinuous Galerkin method using WENO limiters II: Unstructured meshes. *J. Comput. Phys.*, 227(2008)4330-4353.
- [18] D.W. Zingg, S. De Rango, M. Nemeć and T.H. Pulliam, Comparison of several spatial discretizations for the Navier-Stokes equations, *J. Comput. Phys.*, 160(2000)683-704.